◆ Human Brain Mapping 27:47–62(2006) ◆

Method for Multimodal Analysis of Independent Source Differences in Schizophrenia: Combining Gray Matter Structural and Auditory Oddball Functional Data

V.D. Calhoun,[1–3]* T. Adali,[4] N.R. Giuliani,[1] J.J. Pekar,[5,6] K.A. Kiehl[1,2] and G.D. Pearlson,[1–3]

[1]*Olin Neuropsychiatry Research Center, Institute of Living, Hartford, Connecticut*
[2]*Department of Psychiatry, Yale University, New Haven, Connecticut*
[3]*Department of Psychiatry, Johns Hopkins University, Baltimore, Maryland*
[4]*University of Maryland Baltimore County, Department of CSEE, Baltimore, Maryland*
[5]*Department of Radiology, Johns Hopkins University, Baltimore, Maryland*
[6]*FM Kirby Research Center for Functional Brain Imaging, Kennedy Krieger Institute, Baltimore, Maryland*

Abstract: The acquisition of both structural MRI (sMRI) and functional MRI (fMRI) data for a given study is a very common practice. However, these data are typically examined in separate analyses, rather than in a combined model. We propose a novel methodology to perform independent component analysis across image modalities, specifically, gray matter images and fMRI activation images as well as a joint histogram visualization technique. Joint independent component analysis (jICA) is used to decompose a matrix with a given row consisting of an fMRI activation image resulting from auditory oddball target stimuli and an sMRI gray matter segmentation image, collected from the same individual. We analyzed data collected on a group of schizophrenia patients and healthy controls using the jICA approach. Spatially independent joint-components are estimated and resulting components were further analyzed only if they showed a significant difference between patients and controls. The main finding was that group differences in bilateral parietal and frontal as well as posterior temporal regions in gray matter were associated with bilateral temporal regions activated by the auditory oddball target stimuli. A finding of less patient gray matter and less hemodynamic activity for target detection in these bilateral anterior temporal lobe regions was consistent with previous work. An unexpected corollary to this finding was that, in the regions showing the largest group differences, gray matter concentrations were *larger* in patients vs. controls, suggesting that more gray matter may be related to less functional connectivity in the auditory oddball fMRI task. *Hum Brain Mapp 27:47–62, 2006.*

Key words: fMRI; functional; brain; independent component analysis; ICA; schizophrenia; data fusion; gray matter; structural; auditory oddball

Contract grant sponsor: National Institutes of Health; Contract grant numbers: 1 R01 EB 000840-01 (to V.C.); 5 R01 MH43775-08, 5 R01 MH43775-08 (to G.P.).

*Correspondence to: Dr. Vince Calhoun, Olin Neuropsychiatry Research Center, Institute of Living, 200 Retreat Ave., Hartford, CT 06106. E-mail: vince.calhoun@yale.edu

Received for publication 29 October 2004; Accepted 18 April 2005
DOI: 10.1002/hbm.20166
Published online 17 August 2005 in Wiley InterScience (www.interscience.wiley.com).

INTRODUCTION

It is common practice to acquire structural magnetic resonance imaging (sMRI) brain images on the same individuals who also receive functional MRI (fMRI) scans. The sMRI scans are often used to help coregister brains to a common space [Toga and Thompson, 2001], or to enable a surface rendering of the brain for visualization of the fMRI activations anatomic labeling [Corbetta et al., 1998; Van Essen et al., 1998]. Recently, there have been some attempts to utilize structural and functional information jointly (e.g., correlation of structural volumes with functional activation in certain regions) [Hasnain et al., 2001; Wen et al., 2004]. Voxel-based morphometric methods also provide a way to directly compare changes in relative gray matter amounts to changes in fMRI regions by overlapping the statistical maps created from each approach. Such an approach is more appropriately called data integration (or conjunction) as opposed to data fusion (which attempts to analyze both types of information in a joint analysis) [Thomsen et al., 2004].

Although interest is now increasing, little work has been done to examine how changes in brain structure may be associated with changes in fMRI activation across different regions. Because the brain is a vastly interconnected organ, it is reasonable to expect that local changes in brain structure may result in modulations of brain activity in distant regions [Mesulam, 1998]. However, computing such interrelationships is difficult in practice due to the need to examine the relationship between tens of thousands of voxels. Interesting studies have been performed which examine regressions or correlations between gray matter (GM) volumes and fMRI [Siegle et al., 2003] or for relating gray matter homogeneity with fMRI [Mitchell et al., 1988]. Such studies are important, and needed; however, one limitation of such approaches is they do not allow examination of the relationship between all voxels of both fMRI and GM modalities.

Existing tools for examining joint information include region-based approaches such as structural equation modeling or dynamic causal modeling [Friston et al., 2003; McIntosh and Gonzalez-Lima, 1994]. However, these approaches do not provide an examination of the full set of brain voxels. A natural set of tools that avoid this problem include those that transform data matrices into a smaller set of modes or components. Such approaches include those based on singular value decomposition [Friston et al., 1993, 1996; McIntosh et al., 1996] as well as, more recently, independent component analysis (ICA) [McKeown et al., 1998].

Independent component analysis is a statistical and computational technique for revealing hidden factors that underlie sets of random variables, measurements, or signals. ICA has demonstrated considerable promise for the analysis of fMRI [Calhoun et al., 2003; McKeown et al., 2003] and EEG [Makeig et al., 1997] data. Additionally, there have been a few applications of ICA to perfusion [Tasciyan et al., 2001] and structural imaging [Alfano et al., 2002; Nakai et al., 2004] as well.

In this article we introduce the idea of a second-level *feature-based* analysis of an fMRI activation map and a gray matter segmentation map (the features) called "second level" because preprocessing has been performed to generate images which represent features of interest. We utilize a method that enables the decomposition of two features, both collected on every individual, into a joint set of components that are maximally spatially independent components. We recently applied a related approach to perform a joint analysis of *multitask fMRI data* from healthy controls and patients with schizophrenia [Calhoun et al., 2005b]. In this study we apply the same model (with some modifications to generalize the approach) to a dataset of *structural and functional* MRI images. All participants were scanned while performing the auditory oddball fMRI paradigm [Kiehl et al., 2001] and with a high-resolution T_1-weighted scan, used to derive a relative gray matter image. Both auditory oddball functional and gray matter structural maps have been found to show differences in schizophrenia patients. The auditory oddball evoked response is one of the most robust findings in electrophysiology and the associated fMRI involvement reveals robust differences in patients with schizophrenia by activating regions involved in target detection or attentional orienting [Kiehl and Liddle, 2001]. Structural differences are found using both region-of-interest as well as voxel-based morphometry [Giuliani et al., 2005; Pearlson and Marsh, 1999].

Schizophrenia is likely associated with a disruption of the connections present in the healthy brain and particularly involves heteromodal association cortical regions [Andreasen et al., 1999; Lim et al., 1999; Pearlson, 1997; Stevens et al., 1998]. Many studies have found both structural and functional differences by examining fMRI and sMRI data separately. In contrast, a joint analysis would enable one to study the interactions between fMRI and sMRI data. It is reasonable to expect that if schizophrenia is associated with changes in both structural and functional measures, that activation induced by an fMRI task that activates a large network of regions might be related to features of gray matter (in both controls *and* patients, although to different degrees). We thus hypothesized that a small number of joint components would best capture differences between the patients and controls. We expected this network to show decreased activation (diminished functional connectivity) in patients and also to show decreased gray matter concentration. We also expected to find other joint components which showed increased fMRI activation in patients and decreased gray matter concentration (which would suggest structural changes underlying compensatory functional activation).

THEORY

The joint ICA model assumes that joint spatially independent sources are linearly mixed together by a shared mixing parameter a_{ic}. Specifically, we have a set of two equations:

$$x_{i,v}^{(1)} = \sum_{c=1}^{C} a_{ic} s_{c,v}^{(1)} \text{ and } x_{i,v}^{(2)} = \sum_{c=1}^{C} a_{ic} s_{c,v}^{(2)} \quad (1)$$

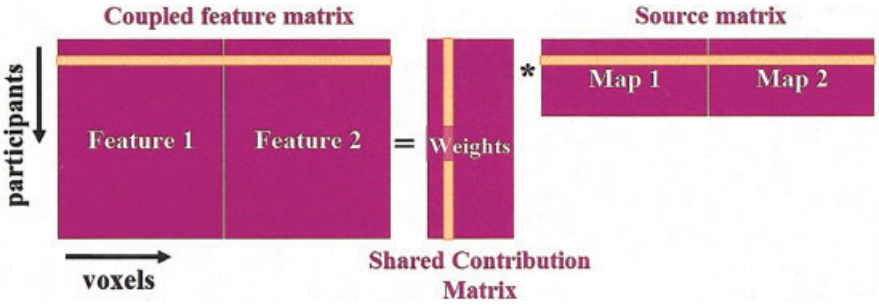

Figure 1.
Model in which loading parameters are shared for the hidden feature/source. The feature matrix is organized by placing the features (SPM map and GM map) from the two modalities side by side. This matrix is then modeled as containing spatially independent joint source images which share common mixing matrix parameters.

where $s_{c,v}^{(k)}$ and $x_{i,v}^{(k)}$ represent the c_{th} independent source and mixed data from individual i for modality k and voxel v, respectively. Alternatively, if we, for the moment, assume we have only one source for each task and write the *unmixing* equations for the two modalities $s_{(2)}$ and $wx_{(2)}$ (where $w = 1/a$), we can write the likelihood functions $p(x_{(1)};w)$ and $p(x_{(2)};w)$, considered as functions of w. If we were to run ICA on each modality separately, we maximize these two likelihood functions in separate ICA analyses. This would result in two sets of optimal unmixing coefficients, $w_1^* = \arg\max_{w_1} \log p(x^{(1)};w_1)$ and $w_2^* = \arg\max_{w_2} \log p(x^{(2)};w_2)$, one for each modality. To interpret both results together, w_1^* and w_2^* would then have to be combined somehow as they are computed independently of one another. If, on the other hand, we utilize a data fusion approach, we determine a single optimal unmixing coefficient that maximizes the joint likelihood function, $w^* = \arg\max_w \log p(x^{(1)},x^{(2)};w)$. It makes intuitive sense *not* to compute the parameters independently, since the activation maps from the two modalities are coming from the same participant. Thus we have a single w^* which fuses the information from two sources (or, alternatively, represents a basis vector common to both). The main advantage of this approach is that maximizing the joint likelihood function provides a different (and more reasonable) solution from one that does not utilize the joint statistics.

We assume the following generative model for the data: $\mathbf{x}^F = \mathbf{A}\mathbf{s}^F$ and $\mathbf{x}^G = \mathbf{A}\mathbf{s}^G$, where, for the case of two sources and two subjects, $\mathbf{x}^F = [x_1^F \quad x_2^F]^T$ is the mixed data for the fMRI modality for the two subjects, $\mathbf{x}^G = [x_1^G \quad x_2^G]^T$ is the mixed data for the gray matter modality for the two subjects, $\mathbf{A} = \begin{bmatrix} a_{11} & a_{12} \\ a_{21} & a_{22} \end{bmatrix}$ is the *shared* mixing matrix, and $\mathbf{s}^F$ and $\mathbf{s}^G$ are the respective fMRI and gray matter sources (note, in the nonjoint case, we would instead have $\mathbf{x}^F = \mathbf{A}\mathbf{s}^F$ and $\mathbf{x}^G = \mathbf{B}\mathbf{s}^G$). We can write this as a single equation by forming a data vector for each subject as $\mathbf{x_i} = [x_i^F \quad x_i^G]$,, and likewise for a source vector $s_i = [s_i^F \quad s_i^G]$. The resulting mixing equation for subject i is then $\mathbf{x}_i = \mathbf{A}\mathbf{s}_i$. One may use existing ICA analysis algorithms to perform a joint analysis by forming the overall data matrix $\mathbf{X} = [\mathbf{X}^{(1)},\mathbf{X}^{(2)}]$, stacking one beside the other (see Fig. 1), and likewise forming $\mathbf{S} = [\mathbf{S}^{(1)},\mathbf{S}^{(2)}]$ in which each of the original image component rows $\mathbf{S}_c^{(1)}$ and $\mathbf{S}_c^{(2)}$ are placed adjacent to form a total combined row of length $2V$ (the number of voxels in two images). (Additional numbers of data types may be handled similarly.) The identification of components with shared loading parameters, and the comparison of the associated maps, is a key means to identify couplings between brain image components of different types of data.

SUBJECTS AND METHODS

Simulations

We examine the behavior of our algorithm by creating a "hybrid" dataset in which a known source is mixed and added to actual AOD and GM data. These data are then unmixed using the algorithm described in the previous section. Since the superimposed sources have a known pattern, it is straightforward to extract them from the unmixed data. Such an approach enables us to evaluate the performance of the jICA algorithm under a variety of noise conditions, using data that have a complex structure (since it is partially comprised of actual data). We can then evaluate the solution, and different models, by comparing the known unmixed sources to the ground truth using a measure such as correlation or KL Divergence, $D(\mathbf{s} \mid \mathbf{u})$, between the known "truth" and the estimated joint sources [Calhoun et al., 2004a].

A hybrid-data experiment was generated (shown in Figure 3) in which a known source (a 21 × 21 half-cycle sinusoid) was added to different parts of a single-slice of auditory oddball and gray matter data from 30 healthy individuals after multiplication by a random number drawn from a uniform distribution (the mixing parameter) with half of the individuals (the patients) having a mean shifted down by 0.5 from the other half of the individuals (the controls). We generated hybrid datasets under a variety of contrast-to-noise ratios (CNRs) by scaling the known source relative to the fMRI and GM data. These data were then entered into a jICA analysis and the component which showed a significant difference between the groups was examined.

Participants

Participants were recruited via advertisements, presentations at local universities, and by word-of-mouth. Fifteen healthy participants and 15 outpatients with chronic schizophrenia, currently in complete or partial remission, provided written, informed, IRB-approved consent at Hartford Hospital and were compensated for their participation. Prior to inclusion in the study, healthy participants were screened

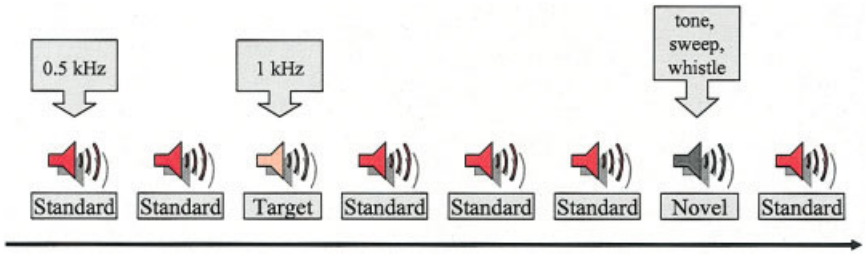

Figure 2.
Auditory oddball paradigm. Auditory oddball event-related fMRI task.

to ensure they were free from DSM-IV Axis I or Axis II psychopathology (assessed using the SCID [Spitzer et al., 1996] and also interviewed to determine that there was no history of psychosis in any first-degree relatives). Patients met criteria for schizophrenia in the DSM-IV on the basis of a SCID diagnosis and review of the case file [First et al., 1995]. All but one of the patients were stabilized on atypical antipsychotic medications. There were equal numbers of males (n = 12/12) and females (n = 3/3) in the patient and control groups and all but two participants in each group were right-handed. There were no significant between-group differences in age (patients 37 ± 11 years; controls 38 ± 11 years). All participants had normal hearing (assessed by self-report) and were able to perform the task successfully during practice prior to the scanning session.

Task

Auditory oddball

The auditory oddball task (AOD) consists of detecting an infrequent sound within a series of regular and different sounds. The task consisted of two runs of auditory stimuli presented to each participant by a computer stimulus presentation system via insert earphones embedded within 30-dB sound-attenuating MR-compatible headphones. The standard stimulus was a 500-Hz tone, the target stimulus was a 1,000-Hz tone, and the novel stimuli consisted of nonrepeating random digital noises (e.g., tone sweeps, whistles) (Fig. 2). The target and novel stimuli each occurred with a probability of 0.10; the nontarget stimuli occurred with a probability of 0.80. The stimulus duration was 200 ms with an 800, 1,300, or 1,800 ms interstimulus interval. All stimuli were presented at ~80 dB above the standard threshold of hearing. All participants reported that they could hear the stimuli and discriminate them from the background scanner noise. The intervals between stimuli of interest (i.e., target and novel stimuli) were allocated in a pseudorandom manner to ensure that these stimuli had equal probability of occurring at 0, 1/3, and 2/3 after the beginning of the image acquisition period. Because of this the hemodynamic response to each type of stimulus of interest was sampled uniformly at 500-ms intervals. Prior to entry into the scanning room, each participant performed a practice block of 10 trials to ensure an understanding of the instructions. The participants were instructed to respond as quickly and accurately as possible with their right index finger every time they heard the target stimulus and not to respond to the nontarget stimuli or the novel stimuli. An MRI-compatible fiber-optic response device (Lightwave Medical, Vancouver, BC) was used to acquire behavioral responses for the task. The stimulus paradigm, data acquisition techniques, and previously found stimulus-related activation are described more fully elsewhere [Kiehl and Liddle, 2001; Kiehl et al., 2004].

Imaging Parameters

Scans were acquired at the Olin Neuropsychiatry Research Center at the Institute of Living on a Siemens Allegra 3T dedicated head scanner equipped with 40 mT/m gradients and a standard quadrature head coil. High-resolution, isotropic T_1-weighted images were acquired using a 3-D MP-RAGE pulse sequence with the following imaging parameters: TR/TE/TI = 2300/2.74/900 ms, flip angle = 8°, field of view (FOV) = 176 × 256 mm, Slab thickness = 176 mm, matrix = 176 × 256 × 176, voxel size = 1 × 1 × 1 mm, number of average = 2, pixel bandwidth = 190 Hz, total scan time = 10:09 min. The functional scans were acquired using gradient-echo echo-planar-imaging with the following parameters (repeat time (TR) = 1.50 s, echo time (TE) = 27 ms, FOV = 24 cm, acquisition matrix = 64 × 64, flip angle = 70°, voxel size = 3.75 × 3.75 × 4 mm, gap = 1 mm, 29 slices, ascending acquisition). Six "dummy" scans were performed at the beginning to allow for longitudinal equilibrium, after which the paradigm was automatically triggered to start by the scanner.

Data Analysis

sMRI: optimized VBM

A study-specific template was created in order to control for intensity differences in MR images based on scanner, template, and population variations using the optimized VBM approach [Good et al., 2001]. First, a whole brain template was created from the images of all participants as follows. Image volumes were first roughly normalized using a 12-parameter affine model to the 152 average T_1 MNI (Montreal Neurological Institute) template SPM T_1 template. Next, images were segmented into gray, white, and cerebrospinal fluid (CSF) compartments and smoothed with an 8-mm smoothing full width at half-maximum (FWHM) kernel. All smoothed segments were then averaged to create T_1, gray, white, and CSF templates. The raw T_1 images were then segmented in their native space and resulting gray

matter images were normalized to the customized gray matter templates. Normalization parameters were recorded and applied to the raw T_1 images. Finally, the warped T_1 images were segmented into individual gray, white, and CSF maps for each subject using a modified mixture-model clustering algorithm [Ashburner and Friston, 2000]. The resulting images are probabilistic segmentations (soft classifications) of gray matter [Ashburner and Friston, 2000]. The addition of the first segmentation step minimizes the number of non-brain voxels misclassified as gray matter (GM) [Good et al., 2001]. Gray matter images were then smoothed with a 12-mm FWHM Gaussian kernel [Good et al., 2001].

fMRI: preprocessing

fMRI data were preprocessed using the software package SPM2 (see http://www.fil.ion.ucl.ac.uk/spm). Images were realigned using INRIalign, a motion correction algorithm unbiased by local signal changes [Freire and Mangin, 2001; Freire et al., 2002]. Data were spatially normalized into the standard MNI space [Friston et al., 1995], spatially smoothed with a $10 \times 10 \times 12$ mm^3 FWHM Gaussian kernel. The data were slightly subsampled to $3 \times 3 \times 3$ mm, resulting in $53 \times 63 \times 46$ voxels. For display, even slices 8–38 are presented.

fMRI: GLM analysis

Data for each subject were analyzed by multiple regression incorporating regressors for the novel, target, and standard stimuli and their temporal derivatives plus an intercept term. Regressors were created by modeling the stimuli as delta functions convolved with the default SPM2 hemodynamic response function. Only correct responses were modeled. The contrast used in the jICA analysis was the AOD target stimuli. The amplitude estimates from the first level analysis were utilized following amplitude bias correction by the derivative terms [Calhoun et al., 2004b].

jICA analysis

The algorithm for the jICA analysis proceeds with the following steps.

Feature selection. An SPM contrast image for AOD targets and a GM segmentation image were computed for each individual.

Feature normalization. Both GM and AOD images were sampled to have a voxel size of (2 mm)^3 and normalized to have the same average sum-of-squares (computed across all subjects and all voxels for each modality). The normalization is needed because the GM and AOD data have different ranges. A single normalization factor is used for each data type; thus, following normalization, the relative scaling within a given data type is preserved, but the units between data types are the same (in a least-squares sense). Additionally, because the gray matter images are only positive valued (between 0 and 1), to preserve this positivity in the analysis (and prevent voxels with near zero gray matter from making a large contribution) the sign was flipped on alternate voxels. This heuristic step was performed such that the mean value of the image would be zero and the large negative and positive values would both be from voxels which had high amounts of gray matter concentration present.

Feature matrix composition. In-brain voxels were analyzed and the two feature datasets were organized into a matrix as in Figure 1.

Dimensionality estimation. We used the Minimum Description Length [Calhoun et al., 2001; Rissanen, 1983] criteria to estimate the dimensionality of the feature matrix.

Dimensionality reduction. PCA was used to reduce the dimensionality of the data down to the estimated dimensionality (from previous step).

Spatial ica decomposition. The infomax algorithm [Bell and Sejnowski, 1995] was used to decompose the reduced feature-matrix to maximally independent component images and subject specific mixing (loading) parameters.

Component selection. Loading parameters were examined for a significant difference between patients and controls using a *t*-test and only significant components were subsequently examined.

Component display. Joint components were reconverted into 3-D images and the initial sign-flipping process was reversed. The joint ICA analysis produces a set of different regions for each type of data (for clarity we call these the jICA-GM and the jICA-AOD regions), an indication which part of the combined data contributed significantly to the source. It is thus possible for the combined maps to have (1) only the AOD part showing large values, (2) only the GM part showing large values, (3) both the AOD and GM parts showing large values.

Because our generative model assumes the same mixing matrix for both modalities, we also examined whether an ICA analysis of each modality separately would produce a similar mixing matrix and, if so, how it would compare with the jointly estimated mixing matrix. We tested this using simulations and also on the fMRI and GM data. First, we generated a simulated set of sources, for two "modalities" combined with a common, randomly generated mixing matrix. We then performed an ICA analysis of one dataset alone, and another ICA analysis using both datasets in a joint analysis. The resulting mixing matrices were then compared to the "true" mixing matrix by sorting the estimated mixing matrix columns according to their correlation with the true mixing matrix and computing the average correlation over all components. This was done multiple times to assess the performance. We also examined performance when computing ICA of one dataset and using this mixing matrix to calculate the "source" from the second dataset by regressing the mixing matrix parameters onto the second

dataset. To assess performance, the average correlation of the regression-estimated sources to the "true" sources was computed. We also examined the results for real data. For this case, we ran an ICA analysis on the normalized AOD data alone and a separate ICA analysis on the normalized GM data alone. The same number of sources estimated from the entire dataset was estimated for these separate analyses. In both cases, we selected the component that was most significantly different for the patient and controls groups and compared the spatial maps.

In addition to examination of the regions contained within the joint source images (Component display, above), because our approach is new we also examined our data in two other ways. First, within the detected regions (jICA-GM and jICA-AOD) we examined the values of a standard random effects SPM (AOD) and VBM (GM) approach for controls vs. patients. The SPM (AOD) result was produced by entering the AOD contrast images into a two-sample *t*-test within the jICA-GM and jICA-AOD regions. The VBM (GM) approach was produced by entering the GM images into a two-sample *t*-test (also within the jICA-GM and jICA-AOD regions). This produces four additional results: SPM and VBM values within jICA-GM and jICA-AOD regions. Finally, we examined the multimodality data using a histogram analysis. Voxels that were significant in the jICA analysis for either of the two data types were used to generate a joint histogram of the AOD and GM data. These histograms were examined in individual participants and as group averages. In the Discussion, we group our results into three subsections reporting on (1) the behavior of the AOD data alone within the jICA-AOD and jICA-GM regions, (2) the behavior of the GM data alone in these two sets of regions, and (3) the joint analysis of both datasets.

RESULTS

Simulations

Results for a hybrid dataset under a higher noise situation (CNR = 0.5), comparable to the size of the signals found in our data, and a lower noise situation (CNR = 1) are shown in Figure 3. The component which showed the largest group difference is displayed with the AOD part of the joint source on the left, the GM part of the joint source in the middle, and the correlation of the loading parameter with the ground truth on the right ("patients" are coded in cyan, "controls" in yellow). In both cases the correct joint component was found and the controls show a lower mean than the patients (as expected). The jICA analysis thus selects out the coupled source into a separate component and enables us to visualize where in each dataset the coupling occurs, as well as the loading parameters.

Behavioral Data

For the auditory oddball task, performance and significances for whether controls and patients differed was as follows: reaction time (controls 431.1 ± 102.2 ms; patients 522.3 ± 162.6 ms, $P < 0.01$), accuracy for target detection (controls 99.6 ± 0.01%; patients 97.7 ± 0.05%, $P > 0.2$).

jICA Analysis

Results from the jICA analysis of both modalities are presented in Figure 4. Ten components were estimated from the data. The AOD part of the joint source is shown in Figure 4a, the GM part of the joint source is shown in Figure 4b, and the ICA loading parameters separated by group are shown in Figure 4c. Only one component was significantly different at the $P < 0.01$ level. This component demonstrated different loadings ($P \sim 0.0012$) in patients and controls (loading for controls was higher than that for patients). Different networks were identified for the fMRI and sMRI data. For display, auditory oddball and gray matter sources were converted to Z-values (by dividing by the standard deviation of the source) and thresholded at $|Z| > 3.5$. The AOD data showed primarily regions with greater activation in healthy controls (including temporal lobe structures and cerebellum) and the GM data showed only regions with smaller concentrations (bilateral frontal and parietal, right temporal) in controls. Talairach coordinates for the AOD and GM jICA analyses are presented in Table I.

Results from our examination of separate ICA vs. joint ICA approaches are summarized as follows. For the simulations, we varied the number of samples (voxels) and randomly generated sources and mixing matrices. In all cases, joint ICA showed slightly improved performance over estimating the mixing matrix from a single dataset. For example, for 10 trials, with a sample size of 10,000 and estimating 10 components, each with lognormal distributions, the joint ICA showed an average correlation of 0.99 ± 0.002, whereas the separate ICA estimation had an average correlation of 0.97 ± 0.004 ($P < 0.002$, two-sample *t*-test). When examining the performance of joint ICA vs. separate ICA plus regression for a different simulation, but with the same parameters just mentioned, the joint ICA showed an average correlation of 0.94 ± 0.05 and the separate ICA plus regression showed an average correlation of 0.88 ± 0.07 ($P < 0.007$, two-sample *t*-test). For another simulation we used 15 trials, with a sample size of 10,000, estimating 10 components with Gaussian distributions (we used Gaussian distributions because in this case the ICA approach is not expected to work as well, since it is not possible in general to separate Gaussian distributions with ICA). In this case, the joint ICA showed an average correlation of 0.84 ± 0.05, whereas the separate ICA analysis had an average correlation of 0.81 ± 0.07 ($P < 0.05$, two-sample *t*-test).

For the analysis of AOD and GM data, separate ICA analyses of each normalized dataset revealed similar, but not identical components which discriminated the groups. The resulting maps are shown in Figure 5 and should be compared with the images in Figure 4. The regions identified are largely similar, which gives us additional confidence in the joint ICA approach. The significance values for the mixing coefficients were slightly higher for the AOD than the GM maps ($P < 0.001$ vs. $P < 0.01$); however, were both

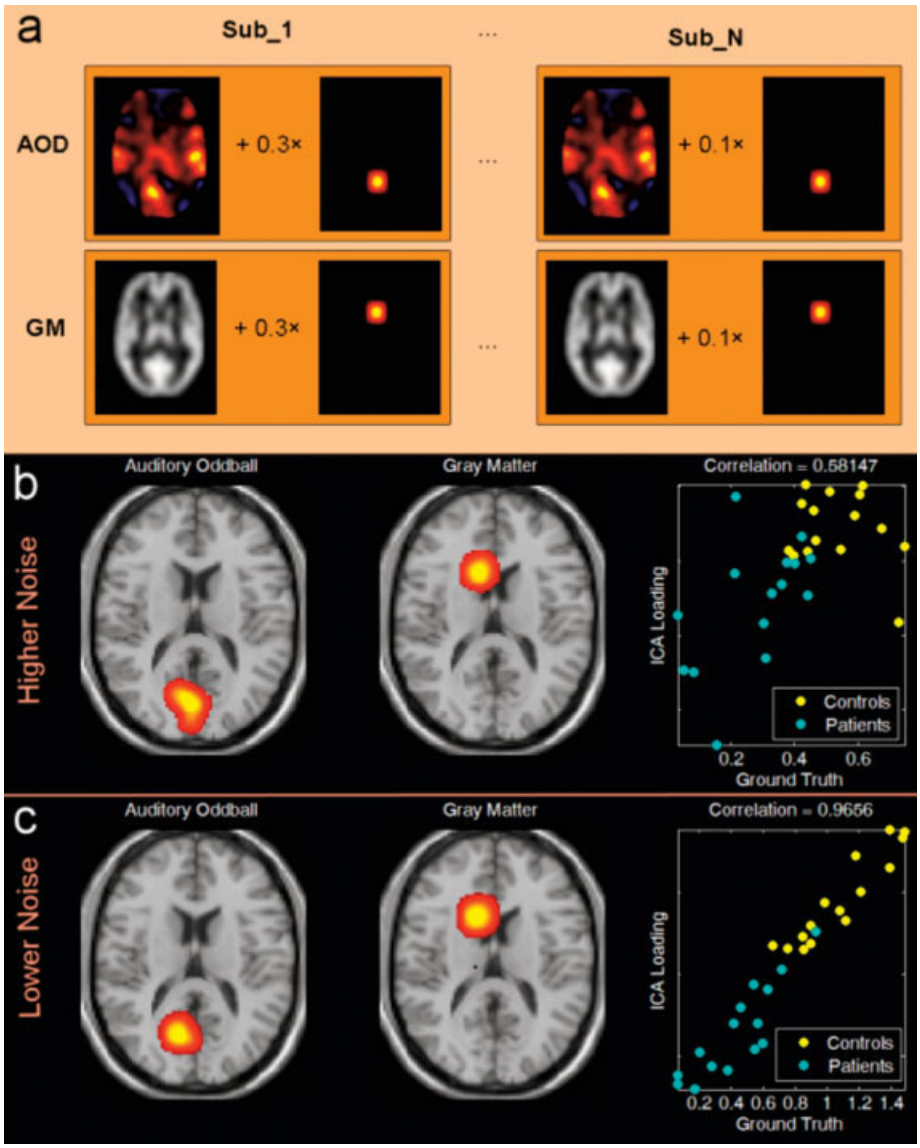

Figure 3.
Simulation and simulation results. Generation of hybrid data is depicted. Results from a lower and higher noise environment is shown in **b,c**. The source which revealed the greatest difference between the two "groups" is shown for the AOD part of the joint source (left, **b,c**) and the GM part of the joint source (middle, **b,c**). Loading parameters vs. the ground truth values are shown on the far right of **b,c**.

still significant. Figure 5 shows the resulting maps if the mixing matrix generated from the separate ICA of AOD analysis is regressed onto the GM data to generate the spatial maps. The correlation between the corresponding mixing matrix columns of the separate ICA analyses and the joint ICA analysis for the AOD and GM data significant component were 0.6 and 0.7, respectively.

We can also examine directly the relationship between the GM and AOD regions. In order to examine the joint task activity in more detail, a joint histogram was computed as follows. Voxels surviving the threshold for the AOD part of the joint source were sorted in descending order using the component voxel values (the same was done for voxels in the GM part of the joint source). This procedure resulted in two sets of voxels coordinates. Histograms were then generated by pairing these two voxel sets. For example, the first two points for individual 1 are the voxels values for the AOD fMRI activation data (at the position that is maximum in the AOD part of the jICA source) vs. the voxel values for the GM segmentation data (at the position which is maximum in the GM part of the jICA source). These pairings were used to generate single-subject 2-D histograms of gray matter concentration vs. AOD fMRI signal. The histogram image for each participant is shown in Figure 6a. In addition, we computed the within-group average of the histograms and subtracted the controls group average from the patient group averaged (shown in Fig. 6b). For the voxels included, the 2-D histogram can be considered an estimate of the joint distribution function for the two modalities (e.g., $p(f_{aod}, f_{gm})$ where $f_{aod,gm}$ indicates the fMRI signal amplitude for the auditory oddball task or the relative gray matter concentration, respectively). We also computed the marginal estimated distributions $p(f_{aod}) = \Sigma_{gm} p(f_{aod}, f_{gm})$ and $p(f_{gm}) = \Sigma_{aod} p(f_{aod}, f_{gm})$ (Fig. 6c,d). The main finding is that

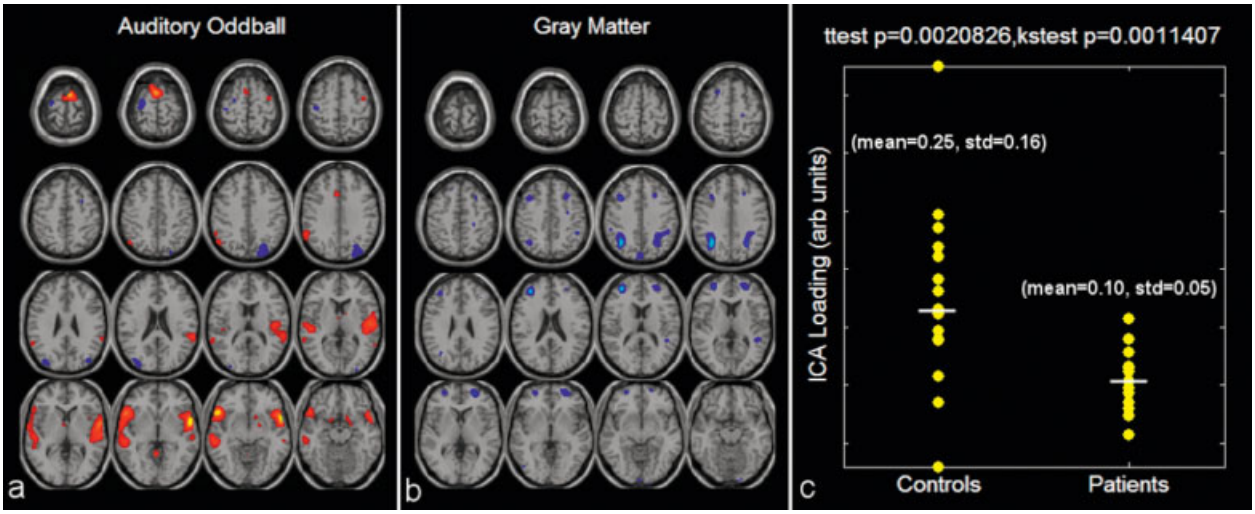

Figure 4.
Auditory oddball/gray matter jICA analysis. Only one component demonstrated a significant difference between patients and controls. The joint source map for the auditory oddball (left) and gray matter (middle) data is presented along with the loading parameters for patients and controls (far right).

healthy controls have increased fMRI activation on the AOD task (in regions shown in Fig. 4a), whereas patients with schizophrenia have increased GM concentration (in regions shown in Fig. 4b). This is visible on both the group average histograms in Figure 6b (the patient histogram is located above and to the left of the control histogram) as well as the plots in Figure 6c (patient plots are to the left for the AOD data and to the right for the GM data). The correlation difference between AOD and GM data at the maximum voxel for the AOD and GM parts of the joint source was $\Delta\rho = 0.52$ ($P < 0.0017$), again suggesting a group difference relationship between AOD and GM in the detected regions.

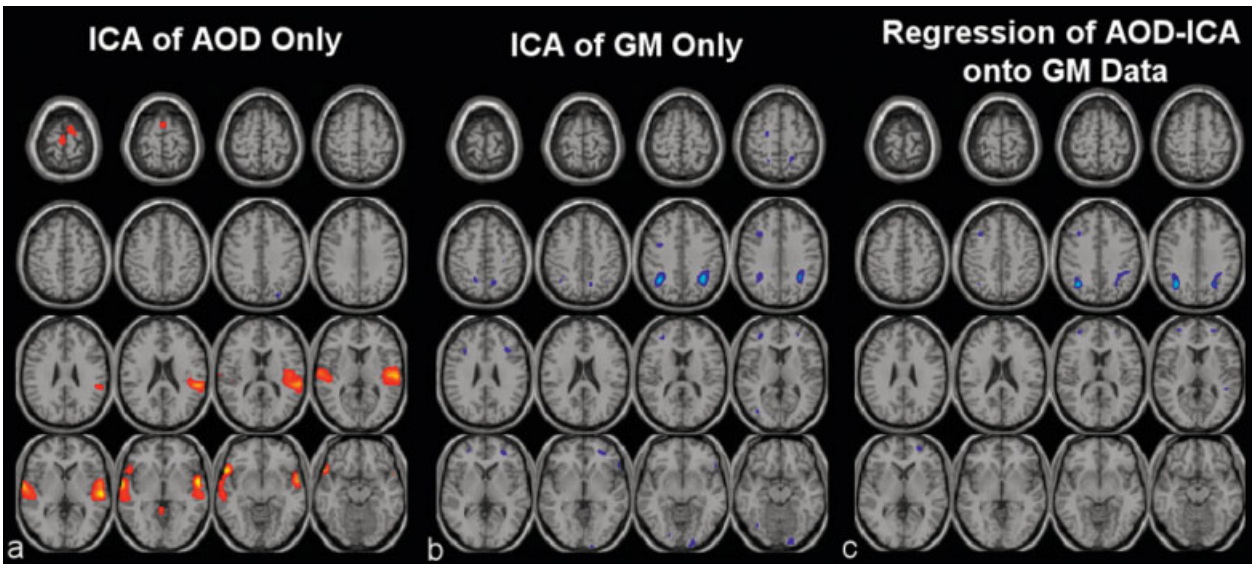

Figure 5.
Separate ICA analyses of GM and AOD data. ICA was used to estimate components for each modality separately from the normalized data. The AOD (**a**) and GM (**b**) results were largely similar to the results found for the joint estimation. This gives us confidence that the assumptions made for the joint analysis are reasonable ones. **c:** The resulting spatial map if the mixing matrix from the separate AOD analysis (**a**) is regressed onto the GM data to generate the spatial map.

TABLE I. Talairach coordinates for the AOD and GM jICA analysis

Area	Brodmann	L/R volume (cc)	L random effects: Max T (x,y,z)	R random effects: Max T (x,y,z)
Auditory oddball				
Control greater				
Superior temporal gyrus	22:*:38:41:21:42:13:29	9.6/12.5	7.6 (−53,17,−9)	9.5 (59,6,−4)
Inferior frontal gyrus	47:*:45	4.4/1.6	8.6 (−53,17,−6)	5.9 (48,17,−8)
Superior frontal gyrus	6:11:10:8	2.9/2.3	8.4 (0,7,66)	8.1 (6,3,70)
Middle temporal gyrus	21:*:22:20:39	4.8/1.3	5.8 (−53,−29,−4)	6.9 (59,2,−7)
Transverse temporal gyrus	42:41	1.2/1.4	5.0 (−48,−25,10)	6.5 (57,−15,8)
Precentral gyrus	6:43:13:44	0.1/1.6	3.8 (−59,12,3)	6.0 (53,−4,6)
Insula	13:40:29:*:22:47	0.7/2.9	4.3 (−42,13,−2)	5.6 (46,−17,12)
Medial frontal gyrus	6:25	0.3/0.1	5.4 (0,3,62)	4.6 (14,3,66)
Postcentral gyrus	43:40:2	0.0/0.8	3.2 (−51,−25,14)	5.2 (51,−15,14)
Middle frontal gyrus	6:10	0.1/0.6	3.1 (−36,56,−3)	5.1 (40,−1,57)
Inferior parietal lobule	40:39:7	1.6/1.1	4.8 (−48,−62,42)	5.0 (59,−34,22)
Posterior cingulate	29:30	0.3/0.1	4.9 (0,−49,1)	4.5 (0,−52,1)
Cingulate gyrus	32:24	0.9/0.1	4.6 (−4,19,30)	3.1 (2,17,32)
Supramarginal gyrus	40	1.6/0.2	4.5 (−55,−47,34)	3.7 (59,−46,19)
Parahippocampal gyrus	37:Amygdala:34	0.2/0.4	3.6 (−16,3,−15)	4.1 (18,−1,−10)
Subcallosal gyrus	34:13:47	0.3/0.2	3.9 (−16,7,−15)	3.6 (18,5,−14)
Basal ganglia		1.2/1.7	3.6 (−4,0,4)	3.9 (20,−2,−8)
Lingual gyrus	18	0.1/0.0	3.7 (−4,−53,−2)	ns
Thalamus		0.4/0.2	3.6 (−2,−5,9)	3.3 (2,−5,9)
Anterior cingulate	24	0.1/0.0	3.5 (−8,23,26)	ns
Angular gyrus	39	0.0/0.0	3.4 (−53,−60,34)	ns
Control less				
Precuneus	19:7:31:39	0.2/3.6	3.2 (−16,−68,48)	5.2 (26,−80,39)
Cuneus	19:7	0.5/0.4	3.8 (−28,−84,26)	4.8 (24,−82,37)
Superior frontal gyrus	6:8	0.9/0.2	4.6 (−24,−8,67)	3.4 (26,12,49)
Superior occipital gyrus	19:39	1.0/0.4	4.5 (−32,−80,26)	3.9 (42,−76,28)
Precentral gyrus	6:4	2.3/0.0	4.5 (−24,−12,67)	ns
Middle temporal gyrus	19:39	0.7/0.2	4.3 (−36,−78,26)	3.7 (42,−72,28)
Middle occipital gyrus	19:18	0.5/0.5	4.1 (−32,−80,22)	3.6 (28,−91,16)
Angular gyrus	39	0.2/0.2	3.6 (−36,−74,30)	4.1 (40,−74,30)
Postcentral gyrus	3:5:7	0.8/0.0	4.1 (−42,−20,56)	ns
Superior parietal lobule	7	0.0/0.4	ns	4.0 (24,−74,44)
Middle frontal gyrus	6	0.5/0.6	3.8 (−26,−7,61)	3.6 (30,8,49)
Paracentral lobule	4:5:6	0.5/0.1	3.5 (−6,−38,63)	3.0 (2,−32,61)
Gray matter				
Control less				
Angular gyrus	39	0.6/0.3	8.3 (−34,−58,36)	5.8 (30,−59,34)
Inferior parietal lobule	40:39:7	2.5/1.5	7.8 (−34,−55,36)	5.9 (32,−45,37)
Precuneus	39:19:7:31	1.4/0.9	7.4 (−34,−62,36)	5.6 (28,−60,36)
Middle frontal gyrus	10:8:9:*:6:46:11	4.8/3.1	7.3 (−32,47,14)	5.7 (28,51,7)
Superior parietal lobule	7	0.5/0.4	6.6 (−30,−58,40)	6.2 (30,−54,38)
Superior frontal gyrus	10:6:11:8:9	1.7/2.1	5.9 (−32,51,14)	6.1 (28,52,1)
Precentral gyrus	9:4:6	1.0/0.4	5.9 (−36,21,36)	3.9 (22,−23,53)
Superior temporal gyrus	39:29:13:41:22:38:42	0.1/1.0	5.9 (−34,−55,32)	5.1 (46,−40,13)
Supramarginal gyrus	40	0.6/0.4	5.6 (−36,−45,34)	4.8 (40,−41,37)
Middle temporal gyrus	39:21	0.2/0.2	5.2 (−30,−55,32)	4.6 (50,−40,13)
Medial frontal gyrus	10:9:6	0.0/0.4	ns	4.6 (24,51,10)
Insula	13	0.0/0.4	ns	4.6 (48,−38,15)
Postcentral gyrus	4:3	0.1/0.1	3.1 (−22,−28,55)	4.1 (24,−25,51)
Lingual gyrus	18:17	0.2/0.2	4.0 (−2,−97,−2)	3.7 (16,−96,−9)
Fusiform gyrus	20	0.0/0.1	3.2 (−40,1,−22)	4.0 (40,1,−22)
Cuneus	19:18:17	0.2/0.1	3.9 (0,−82,39)	3.6 (16,−101,−2)
Middle occipital gyrus	19:37	0.1/0.0	3.8 (−44,−72,4)	ns
Inferior temporal gyrus	20:19:*	0.1/0.0	3.4 (−46,−74,2)	3.5 (44,−3,−18)

Voxels above the threshold for Figure 4 were converted from MNI to Talairach coordinates and entered into a database to provide anatomic and functional labels for the left (L) and right (R) hemispheres. Both auditory oddball (top) and gray matter (bottom) voxels are reported. The volume of activated voxels in each area is provided in cubic centimeters (cc). Within each area, the maximum t value and its coordinate are provided.

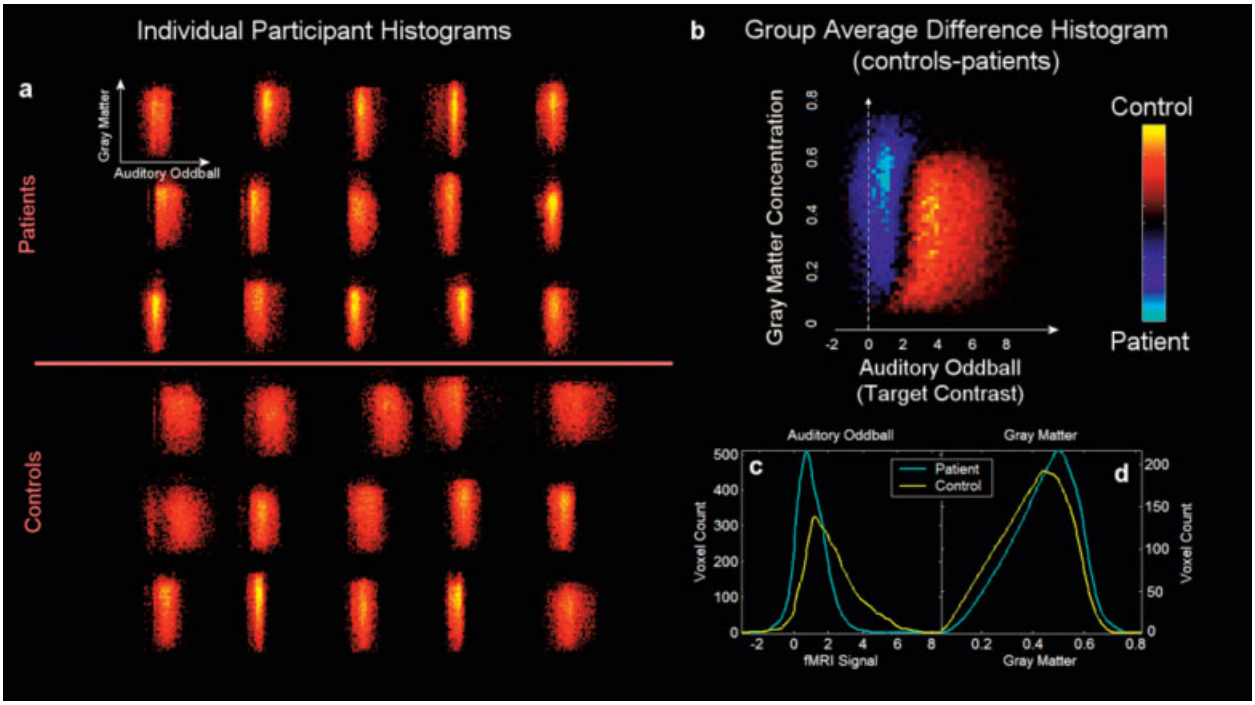

Figure 6.

Cross-modality 2-D histograms. Joint 2-D histograms for voxels identified in the jICA analysis. Individual (**a**) and group average difference (**b**) histograms are provided along with the marginal histograms for the auditory oddball (SPM contrast image) (**c**) and gray matter (segmented) (**d**) data. In the marginal histograms it is clear that controls (yellow) tend to have higher auditory oddball fMRI activation, whereas patients (cyan) tend to have higher gray matter values.

To further investigate the results, we also examined the AOD and GM maps with standard voxel-based analyses. In Figure 7 we mask the SPM difference images for controls vs. patients with the regions which were revealed by the jICA analysis for the joint AOD source (not outlined) and the joint GM source (outlined in white) regions. Figure 7a shows the T-values from the AOD data and Figure 7b shows the T-values from the GM data. The AOD fMRI activation values (Fig. 7a) are positive (greater) for healthy controls (orange/red) in areas contributing to the AOD joint source and also

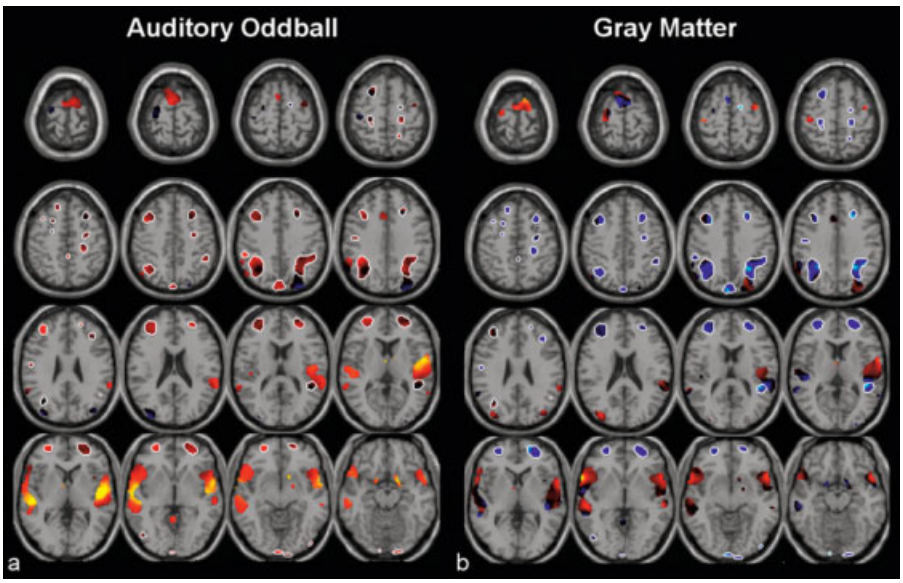

Figure 7.

Auditory oddball/gray matter group difference maps. Standard SPM/VBM difference maps (controls minus patients) for the auditory oddball (left) and gray matter (right) data masked by the jICA-GM regions (outlined in white) and the jICA-AOD regions. Controls demonstrated more activation relative to patients in a variety of regions for the AOD tasks (consistent with previous findings) and demonstrated increased left DLPFC and decreased basal ganglia activation (also consistent with previous findings). The GM values are increased in controls for the jICA-AOD regions and decreased for the jICA-GM regions.

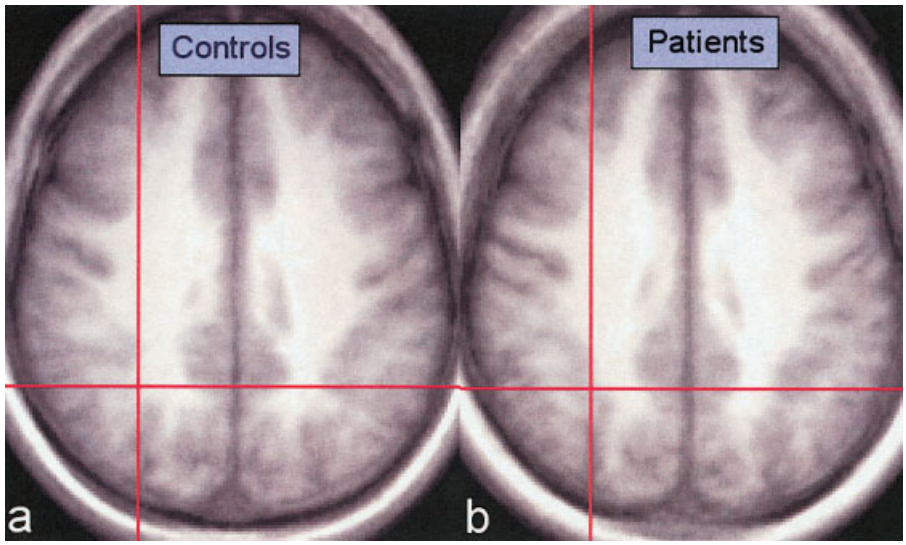

Figure 8.
Average T_1-weighted images for healthy controls and patients with schizophrenia. The crosshair is positioned at the region showing largest gray matter increase in patients. This view clearly shows more gray matter in patients.

largely positive for area contributing to the GM joint source. In contrast, the GM concentration differences are largely positive (greater) for healthy controls for areas contributing to the AOD joint source but negative (smaller) for healthy controls in regions contributing to the GM joint source.

Because our finding of more gray matter in schizophrenia was not expected, we also examined the mean images from each group in the parietal region demonstrating the largest change. Figure 8a shows the control average and Figure 8b shows the patient average. The cursor is placed at the location of interest, and clearly shows more gray matter in that portion of the parietal lobe. As an additional check, we examined the same voxel in a previously published VBM study with approximately twice the sample size and found similar larger patient vs. control gray matter concentrations (although it did not meet the significance criteria set for the study) [Giuliani et al., 2005]. We discuss this finding further in the next section.

DISCUSSION

We have demonstrated an approach for analyzing fMRI data and gray matter (GM) segmentation data in a unified framework using joint independent component analysis (jICA). An analysis of data from healthy controls and patients with schizophrenia revealed several interesting findings. The main finding was that the jICA results identified group differences in bilateral parietal and frontal as well as right temporal regions in gray matter associated with bilateral temporal regions activated by the auditory oddball (AOD) target stimulus. This finding suggests gray matter regions that may serve as a morphological substrate for *changes* in (functional) connectivity as probed by the AOD target stimuli (although we cannot at this time assess the causality of the GM or AOD changes). An unexpected corollary to this finding was that, in the regions showing the largest group differences, GM concentrations were *greater* in patients vs. controls, suggesting that greater GM is related to less functional connectivity in the AOD fMRI task.

Since the joint ICA analysis produces a set of different regions for each type of data (for clarity we call these the jICA-GM and the jICA-AOD regions), we examined the behavior of the AOD or GM data in both sets of regions. Because our analysis is not a standard one, it is helpful to break it into several subsections for discussion. We start by discussing the behavior of the AOD data alone within the jICA-AOD and jICA-GM regions, followed by a discussion of the behavior of the GM data alone in these two sets of regions. Finally, we propose some possible interpretations of the joint analysis of both datasets.

Auditory Oddball Target Response

Both the jICA-AOD and the jICA-GM regions revealed, consistent with previous results, more AOD activation in controls than in patients. The jICA-AOD regions, largely a subset of the regions which are strongly activated by the AOD task in previous studies [Kiehl et al., 2004a], were more significantly activated in controls vs. patients [Kiehl and Liddle, 2001; Stevens et al., 2000]. Kiehl and Liddle [2001] also show excessive target-related activity in posterior temporal lobe regions in schizophrenia, suggesting a possible anterior posterior temporal lobe disconnection. Such a division would also be consistent with work that has found changes in source localization in temporal lobe regions [Reite et al., 1989]. In general, patients with schizophrenia have been found to show widespread lesser AOD fMRI activation [Kiehl and Liddle, 2001; Stevens et al., 1998], also consistent with our findings.

Gray Matter Concentration

Consistent with hypotheses, the jICA-AOD regions, a subset of those typically found in previous VBM analyses of controls and patients with schizophrenia [Giuliani et al.,

2005; Hulshoff Pol et al., 2001], showed more GM in patients compared to controls. These regions included large portions of temporal lobe and are consistent with those found in previous work [McCarley et al., 1993]. Other work has found associations between P3 ERP data and GM volumes in frontal and parietal regions under different attentional states [Ford et al., 1994]. Our findings show, for patients relative to controls, less GM in the anterior temporal lobe and more GM in the posterior temporal lobe.

Contrary to our hypotheses, the jICA-GM regions demonstrated *more* GM concentration in patients. At least two previous studies have found more GM in patients with schizophrenia: one in bilateral parietal regions [Suzuki et al., 2002] and another in the supramarginal gyrus [Buchanan et al., 2004]. Another study found less bilateral frontal white matter in first-episode patients [Paillere-Martinot et al., 2001]. A recent DTI study found lower fractional anisotropy values in parietotemporal regions (more on the left than the right) for schizophrenia patients experiencing auditory hallucinations [Hubl et al., 2004]. This is consistent with the increased GM regions found in the current study (also more on the left than the right). Other studies have examined GM concentration changes but have reported primarily less GM in patients [Job et al., 2002; Kubicki et al., 2002; Wilke et al., 2001].

The ICA analyses of each modality separately revealed largely similar findings to the joint analysis. A natural question that arises is "Why not just compute the ICA maps separately?" since to do a joint ICA estimation may impose some additional assumptions on the data. There are, however, several reasons to perform a joint estimation. First, since the results were largely similar, this gives us confidence that our assumption of a common underlying linear mixture for both data types is a reasonable one. Then, even though there are additional assumptions imposed by the joint approach, it uses all available data (data from both modalities) in the estimation of the same number of parameters compared to performing separate ICA steps, hence potentially improving the estimates. This is also supported by our simulation results that show an improvement in performance for the joint ICA approach. However, a more important advantage of the joint approach is that if ICA is used on one modality only, it is not readily apparent how to generate the spatial maps for the more general case of multiple components and multiple modalities. One possibility for computing the maps would be to simply assume the mixing matrix is fixed and to generate spatial maps for the second modality using the mixing matrix produced by ICA of the first modality. However, this is not straightforward, since the data reduction step is different for the GM data, as is the scaling and ordering of the mixing matrix columns. A second possibility is that two separate ICA analyses could be performed as we did above and the mixing coefficients combined (or fused) somehow. The separately estimated maps could then simply be used for interpretation. While this can be done by normalizing and adjusting the sign of each mixing matrix column (to remove the scaling and sign ambiguity in ICA) followed by averaging the mixing matrix columns, this becomes increasingly difficult and ad hoc for noisy data and if more than one column is to be interpreted. And, finally, since we hope to extend our approach to more than two data types, separately estimating and combining additional modalities can quickly become an intractable problem. For the above reasons, estimation of a single mixing matrix using data from both modalities is quite attractive.

The current analysis is fundamentally different from previous methods since both fMRI and GM data were examined. In addition, ICA is a multivariate technique as opposed to voxel-based morphometric approaches based on the univariate general linear model [Friston and Ashburner, 2004]. Although we can clearly see the greater GM in patients in the averaged raw data (Fig. 8) and in separate data from a previous study [Giuliani et al., 2005], these GM differences appear to be highly variable between individuals and may not be well modeled by a univariate VBM approach. In contrast, the jICA approach has a separate loading parameter for each individual and pools information across voxels, which may thus better capture individual variability. In addition, because this is a joint analysis, the variation of the GM regions is detected in the context of its linear relationship to the auditory oddball activation (i.e., it is "fused" to a map containing GM regions). We now discuss the implications of a joint statistical model.

Joint Auditory Oddball fMRI and Relative GM Concentration

The main purpose of the joint ICA method utilized here is to extract the spatial modes of joint, multimodal brain sources that differ in patients and controls. Such an approach requires acceptance of the likelihood of GM differences being related to functional activation. This is not a difficult premise when considering the same set of voxels [Thomsen et al., 2004], or even adjacent voxels [Meyer-Lindenberg et al., 2004], but as the current study shows it also requires the acceptance of related GM regions and functional regions which are spatially *remote*. We suggest that this, also, is a reasonable conception for the relationship between structural and functional differences. In the context of the auditory oddball task, recent hemodynamic imaging studies have shown that processing of low-probability task-relevant "target" stimuli (i.e., oddballs) elicit widespread activity in diverse, spatially distributed cortical and subcortical systems [Kiehl et al., 2005]. The anterior temporal lobe findings are consistent with the work of both McCarley et al. [1993] and Ford et al. [1994] using ERP and sMRI, whereas the anterior/posterior difference in temporal lobe GM changes support the finding of Kiehl and Liddle [2001] using fMRI. Our results thus support and significantly extend previous work.

Schizophrenia is thought to be a disease involving impaired brain connectivity [Friston, 1999]. There have been a number of models proposed, with many studies implicating regions in temporal lobe, cerebellum, thalamus, basal gan-

glia, and lateral frontal regions [Andreasen et al., 1998; Braver et al., 1999; Friston, 1999; McCarley et al., 1991; Weinberger, 1987]. Discoordination models [Andreasen et al., 1998] as well as frontotemporal disconnection models [Liddle et al., 1992] have been suggested. The current analysis reveals a structural–functional network which includes many of the regions mentioned above and the findings are consistent with both the cognitive dysmetria and frontotemporal disconnection models. However, more studies are needed, with increased numbers of patients and controls, to confirm this result.

Our proposed method has several advantages. First, our approach enables the joint analysis of different types of data in a unified analytic framework. This enables an investigator to explore the relationship between functional and structural image data. Second, we utilize a feature-based approach providing a straightforward way to take advantage of data modeled at the first level. These features are then queried for shared dependence, which is not detectable with a simple voxel-wise subtractive or conjunctive approach. Finally, the shared mixing coefficient provides a way to examine individual or group differences in coupling. For the present, we have chosen a priori to analyze only the component(s) that revealed a statistical difference between the two groups. In future work it would be interesting to develop approaches for understanding the full ICA decomposition (e.g., to examine all the components). Additionally, given previous interest in laterality differences in schizophrenia, it would be interesting to examine the laterality of these joint sources.

While the modeling assumptions inherent in ICA have been explored to some degree for fMRI data [McKeown and Sejnowski, 1998] this has yet to be explored for our jICA approach. The main assumptions we make are: (1) independence of the brain networks for the combined AOD and GM data; (2) a linear relationship between the subjects and these networks via the mixing parameters; and (3) the assumption of a common distributional form for the AOD and GM joint sources. The first assumption has been used with good success with brain data previously, and, despite the fact that brain regions are not functioning independently, due to the large number of brain regions and the scarcity of the sources, the independence assumption does appear to have some value. The linear relationship between subjects restated is that we assume common networks/sources, present in all subjects to (linearly) varying degrees. In this study we tested the hypothesis that patients and controls show differing network strengths, and found one component that is consistent with this hypothesis. The third assumption of a common joint-distribution for AOD and GM sources is a sensible thing to do if one is interested in the examination of joint information. However, these assumptions are possibly too limiting in several ways. First, the AOD and GM distributions may need to be modeled explicitly with different marginal distributions. To mitigate this concern in this initial jICA approach, we (1) normalize the AOD and GM data, and (2) utilize the extended infomax algorithm that adaptively models the sources as having either supergaussian (e.g., a distribution with positive kurtosis) or subgaussian distribution. This algorithm has shown to be quite robust to violations of the underlying model for a wide variety of data types [Lee et al., 1999] and enables some flexibility in the source distributions. This is confirmed in our own data since upon examination of the distributions of the joint sources we find that the distribution of the AOD and GM parts of the same source do show some variation (they have different means, variances, etc.), which is to be expected for these data. Finally, the linearity of the subject-wise contribution is an assumption of convenience, which, although it has worked very well thus far for ICA of many different data types, we would like to relax in future work since it is possible that the joint-sources may also show nonlinear relationships.

Additional approaches can be used to provide information about how the AOD and GM data are related. For example, one could perform an ICA analysis of a single modality, and then perform a regression of a selected component's mixing parameters upon the other modality. However, such an approach makes an assumption of directionality in the analysis, which may or may not be appropriate. In our case, since both AOD and GM data have been shown to exhibit differences in patients vs. controls, and there has yet been no direct examination of the correlations between the two, it is not clear which modality should be used as the starting point (nor do we believe that, at least with our data, it is possible to show causality of the observed changes). We did examine ICA maps of each modality separately, and in both cases found a component that was similar, but not identical, to that revealed in our joint ICA analysis. Regression of the corresponding loading parameters on the other modality reveals a map that is similar, but not identical, to that found in our joint ICA analysis. This provides additional confidence in the changes that we are reporting. However, it also illustrates the main point we are trying to convey about the benefits of joint estimation. For this subsequent analysis, we have two sets of loading parameters, components, and a regression image but do not know how to combine them. Finally, there are some small, but significant, differences in the maps produced on each modality separately and those produced by a regression approach (indeed, even if we do a regression on the *same* data, the maps are slightly different). This is not surprising due to modeling differences and also since an approach, based on ICA of the AOD data, for example, would completely ignore the two possibilities of (1) GM changes being most significant, and (2) AOD and GM both significantly influencing the linear combinations.

There are also some additional limitations to the joint ICA approach which should be mentioned. The current framework, for practical reasons, assumes that both voxels and features are independent and identically distributed. Indeed, most ICA models used make this assumption and perform quite well despite the known spatial correlation between voxels (provided appropriate data reduction is utilized [Hyvarinen et al., 2001]). Nonetheless, it can be poten-

tially useful to incorporate some additional prior information on the voxels (such as spatial correlation) as well as incorporate more flexible distributions for different features into the model (e.g., the AOD data and the GM data may be modeled as having different variances, etc.). Additionally, although we have demonstrated some evidence supporting the usefulness of our model, our choice of modeling the shared dependence between the modalities with the mixing parameters should be examined in more studies before the true utility of this assumption will be known. One final point that should not be ignored is that, given the heterogeneity of the structural and functional findings in schizophrenia, it is important to address issues of statistical power for a joint analysis, which may be different than for an individual analysis. This is especially important if findings from a joint analysis are to become clinically relevant. We will attempt to address these limitations in future work.

CONCLUSIONS

We used a joint-ICA model to examine linearly related fMRI auditory oddball target activation data and GM segmentation data. A single component that was significantly different between patients with schizophrenia and healthy controls was examined. GM regions in bilateral parietal lobe and frontal lobe as well as right temporal lobe were found to be associated with auditory oddball activations in bilateral temporal lobe. These findings suggest a possible morphological substrate for auditory oddball connectivity changes in schizophrenia. In general, we suggest that studying interactions between GM data and fMRI data provides a useful way to examine structure and function.

ACKNOWLEDGMENTS

We thank the research staff at the Olin Neuropsychiatry Research Center who helped collect and process the data and Bruce Wexler for helpful comments.

REFERENCES

Alfano B, Amato U, Antoniadis A, Larobina M (2002): Segmentation of MR brain images through discriminant analysis. Italy: Report RT262/02.

Andreasen NC, Paradiso S, O'Leary DS (1998): "Cognitive dysmetria" as an integrative theory of schizophrenia: a dysfunction in cortical-subcortical-cerebellar circuitry? Schizophr Bull 24:203–218.

Andreasen NC, Nopoulos P, O'Leary DS, Miller DD, Wassink T, Flaum M (1999): Defining the phenotype of schizophrenia: cognitive dysmetria and its neural mechanisms. Biol Psychiatry 46:908–920.

Ashburner J, Friston KJ (2000): Voxel-based morphometry—the methods. NeuroImage 11:805–821.

Bell AJ, Sejnowski TJ (1995): An information maximisation approach to blind separation and blind deconvolution. Neural Comput 7:1129–1159.

Braver TS, Barch DM, Cohen JD (1999): Cognition and control in schizophrenia: a computational model of dopamine and prefrontal function. Biol Psychiatry 46:312–328.

Buchanan RW, Francis A, Arango C, Miller K, Lefkowitz DM, McMahon RP, Barta PE, Pearlson GD (2004): Morphometric assessment of the heteromodal association cortex in schizophrenia. Am J Psychiatry 161:322–331.

Calhoun VD, Adali T, Pearlson GD, Pekar JJ (2001): A method for making group inferences from functional MRI data using independent component analysis. Hum Brain Mapp 14:140–151.

Calhoun VD, Adali T, Hansen JC, Larsen J, Pekar JJ (2003): ICA of fMRI: an overview. Proc Int Conf ICA BSS; Nara, Japan.

Calhoun VD, Adali T, Pearlson GD (2004a): Independent components analysis applied to fMRI data: a generative model for validating results. J VLSI Signal Proc Systems 37:281–291.

Calhoun VD, Stevens M, Pearlson GD, Kiehl KA (2004b): fMRI analysis with the general linear model: removal of latency-induced amplitude bias by incorporation of hemodynamic derivative terms. Neuroimage 22:252–257.

Calhoun VD, Kiehl KA, Pearlson GD (2005): A method for multitask fMRI data fusion applied to schizophrenia. Neuroimage 26:S1.

Corbetta M, Akbudak E, Conturo TE, Snyder AZ, Ollinger JM, Drury HA, Linenweber MR, Petersen SE, Raichle ME, Van E, Shulman GL (1998): A common network of functional areas for attention and eye movements. Neuron 21:761–773.

First MB, Spitzer RL, Gibbon M, Williams JBW (1995): Structured clinical interview for DSM-IV axis I disorders-patient edition (SCID-I/P, v. 2.0): New York: Biometrics Research Department, New York State Psychiatric Institute.

Ford JM, Sullivan EV, Marsh L, White PM, Lim KO, Pfefferbaum A (1994): The relationship between P300 amplitude and regional gray matter volumes depends upon the attentional system engaged. Electroencephalogr Clin Neurophysiol 90: 214–228.

Freire L, Mangin JF (2001): Motion correction algorithms may create spurious brain activations in the absence of subject motion. Neuroimage 14:709–722.

Freire L, Roche A, Mangin JF (2002): What is the best similarity measure for motion correction in fMRI time series? IEEE Trans Med Imaging 21:470–484.

Friston KJ (1999): Schizophrenia and the disconnection hypothesis. Acta Psychiatr Scand Suppl 395:68–79.

Friston KJ, Ashburner J (2004): Generative and recognition models for neuroanatomy. Neuroimage 23:21–24.

Friston KJ, Frith CD, Liddle PF, Frackowiak RS (1993): Functional connectivity: the principal-component analysis of large (PET) data sets. J Cereb Blood Flow Metab 13:5–14.

Friston K, Ashburner J, Frith CD, Poline JP, Heather JD, Frackowiak RS (1995): Spatial registration and normalization of images. Hum Brain Mapp 2:165–189.

Friston K, Poline JP, Strother S, Holmes A, Frith CD, Frackowiak RS (1996): A multivariate analysis of PET activation studies. Hum Brain Mapp 4:140–151.

Friston KJ, Harrison L, Penny W (2003): Dynamic causal modelling. Neuroimage 19:1273–1302.

Giuliani N, Calhoun VD, Pearlson GD, Francis A, Buchanan RW (2005): Voxel-based morphometry versus regions of interest: a comparison of two methods for analyzing gray matter disturbances in schizophrenia. Schizophr Res 74:135–147.

Good CD, Johnsrude IS, Ashburner J, Henson RN, Friston KJ, Frackowiak RS (2001): A voxel-based morphometric study of ageing in 465 normal adult human brains. Neuroimage 14:21–36.

Hasnain MK, Fox PT, Woldorff MG (2001): Structure—function spatial covariance in the human visual cortex. Cereb Cortex 11:702–716.

Hubl D, Koenig T, Strik W, Federspiel A, Kreis R, Boesch C, Maier SE, Schroth G, Lovblad K, Dierks T (2004): Pathways that make voices: white matter changes in auditory hallucinations. Arch Gen Psychiatry 61:658–668.

Hulshoff Pol HE, Schnack HG, Mandl RC, van Haren NE, Koning H, Collins DL, Evans AC, Kahn RS (2001): Focal gray matter density changes in schizophrenia. Arch Gen Psychiatry 58:1118–1125.

Hyvarinen A, Karhunen J, Oja E (2001): Independent component analysis. New York: Johns Wiley & Sons. p 1–481.

Job DE, Whalley HC, McConnell S, Glabus M, Johnstone EC, Lawrie SM (2002): Structural gray matter differences between first-episode schizophrenics and normal controls using voxel-based morphometry. Neuroimage 17:880–889.

Kiehl KA, Liddle PF (2001): An event-related functional magnetic resonance imaging study of an auditory oddball task in schizophrenia. Schizophr Res 48:159–171.

Kiehl KA, Laurens KR, Duty TL, Forster BB, Liddle PF. (2001): An event-related fMRI study of visual and auditory oddball tasks. J Psychophysiol 15:221–240.

Kiehl KA, Stevens M, Stevens M, Laurens KR, Pearlson GD, Calhoun VD, Liddle PF (2004a): The amygdala as a salience detector: evidence from a large-scale study (n = 100) of auditory target detection. Hum Brain Mapp (in press).

Kiehl KA, Stevens M, Laurens KR, Pearlson GD, Calhoun VD, Liddle PF (2005): An adaptive reflexive processing model of neurocognitive function: supporting evidence from a large scale (n = 100) fMRI study of an auditory oddball task. Neuroimage 25:899–915.

Kubicki M, Shenton ME, Salisbury DF, Hirayasu Y, Kasai K, Kikinis R, Jolesz FA, McCarley RW (2002): Voxel-based morphometric analysis of gray matter in first episode schizophrenia. Neuroimage 17:1711–1719.

Lee TW, Girolami M, Sejnowski TJ (1999): Independent component analysis using an extended infomax algorithm for mixed subgaussian and supergaussian sources. Neural Comput 11:417–441.

Liddle PF, Friston KJ, Frith CD, Hirsch SR, Jones T, Frackowiak RS (1992): Patterns of cerebral blood flow in schizophrenia. Br J Psychiatry 160:179–186.

Lim KO, Hedehus M, Moseley M, de Crespigny A, Sullivan EV, Pfefferbaum A (1999): Compromised white matter tract integrity in schizophrenia inferred from diffusion tensor imaging. Arch Gen Psychiatry 56:367–374.

Makeig S, Jung TP, Bell AJ, Ghahremani D, Sejnowski TJ (1997): Blind separation of auditory event-related brain responses into independent components. Proc Natl Acad Sci U S A 94:10979–10984.

McCarley RW, Faux SF, Shenton ME, Nestor PG, Adams J (1991): Event-related potentials in schizophrenia: their biological and clinical correlates and a new model of schizophrenic pathophysiology. Schizophr Res 4:209–231.

McCarley RW, Shenton ME, O'Donnell BF, Faux SF, Kikinis R, Nestor PG, Jolesz FA (1993): Auditory P300 abnormalities and left posterior superior temporal gyrus volume reduction in schizophrenia. Arch Gen Psychiatry 50:190–197.

McIntosh AR, Gonzalez-Lima F (1994): Structural equation modeling and its application to network analysis in functional brain imaging. Hum Brain Mapp 2:2–22.

McIntosh AR, Bookstein FL, Haxby JV, Grady CL (1996): Spatial pattern analysis of functional brain images using partial least squares. Neuroimage 3:143–157.

McKeown MJ, Sejnowski TJ (1998): Independent component analysis of fMRI data: examining the assumptions. Hum Brain Mapp 6:368–372.

McKeown MJ, Makeig S, Brown GG, Jung TP, Kindermann SS, Bell AJ, Sejnowski TJ (1998): Analysis of fMRI data by blind separation into independent spatial components. Hum Brain Mapp 6:160–188.

McKeown MJ, Hansen LK, Sejnowsk TJ (2003): Independent component analysis of functional MRI: what is signal and what is noise? Curr Opin Neurobiol 13:620–629.

Mesulam MM (1998): From sensation to cognition. Brain 121:1013–1052.

Meyer-Lindenberg A, Kohn P, Mervis CB, Kippenhan JS, Olsen RK, Morris CA, Berman KF (2004): Neural basis of genetically determined visuospatial construction deficit in Williams syndrome. Neuron 43:623–631.

Mitchell DG, Vinitski S, Burk DL Jr, Levy DW, Rifkin MD (1988): Motion artifact reduction in MR imaging of the abdomen: gradient moment nulling versus respiratory-sorted phase encoding. Radiology 169:155–160.

Nakai T, Muraki S, Bagarinao E, Mikulis DJ, Takehara Y, Matsuo K, Kato C, Sakahara H, Isoda H (2004): Application of independent component analysis to magnetic resonance imaging for enhancing the contrast of gray and white matter. Neuroimage 12:251–260.

Paillere-Martinot M, Caclin A, Artiges E, Poline JB, Joliot M, Mallet L, Recasens C, ttar-Levy D, Martinot JL (2001): Cerebral gray and white matter reductions and clinical correlates in patients with early onset schizophrenia. Schizophr Res 50:19–26.

Pearlson GD (1997): Superior temporal gyrus and planum temporale in schizophrenia: a selective review. Prog Neuropsychopharmacol Biol Psychiatry 21:1203–1229.

Pearlson GD, Marsh L (1999): Structural brain imaging in schizophrenia: a selective review. Biol Psychiatry 46:627–649.

Reite M, Teale P, Goldstein L, Whalen J, Linnville S (1989): Late auditory magnetic sources may differ in the left hemisphere of schizophrenic patients. A preliminary report. Arch Gen Psychiatry 46:565–572.

Rissanen J (1983): A universal prior for integers and estimation by minimum description length. Ann Stat 11:416–431.

Siegle GJ, Konecky RO, Thase ME, Carter CS (2003): Relationships between amygdala volume and activity during emotional information processing tasks in depressed and never-depressed individuals: an fMRI investigation. Ann N Y Acad Sci 985:481–484.

Spitzer RL, Williams JB, Gibbon M (1996): Structured clinical interview for DSM-IV: non-patient edition (SCID-NP): New York: Biometrics Research Department, New York State Psychiatric Institute.

Stevens AA, Goldman-Rakic PS, Gore JC, Fulbright RK, Wexler BE (1998): Cortical dysfunction in schizophrenia during auditory word and tone working memory demonstrated by functional magnetic resonance imaging. Arch Gen Psychiatry 55: 1097–1103.

Stevens AA, Skudlarski P, Gatenby JC, Gore JC (2000): Event-related fMRI of auditory and visual oddball tasks. Magn Reson Imaging 18:495–502.

Suzuki M, Nohara S, Hagino H, Kurokawa K, Yotsutsuji T, Kawasaki Y, Takahashi T, Matsui M, Watanabe N, Seto H, Kurachi M (2002): Regional changes in brain gray and white matter in patients with schizophrenia demonstrated with voxel-based analysis of MRI. Schizophr Res 55:41–54.

Tasciyan TA, Beckmann CF, Morris ED, Smith SM (2001): ICA-based segmentation of the brain on perfusion data. Proc EMBS; Istanbul, Turkey.

Thomsen T, Specht K, Hammar A, Nyttingnes J, Ersland L, Hugdahl K (2004): Brain localization of attentional control in different age groups by combining functional and structural MRI. Neuroimage 22:912–919.

Toga AW, Thompson PM (2001): Maps of the brain. Anat Rec 265:37–53.

Van Essen DC, Drury HA, Joshi S, Miller MI (1998): Functional and structural mapping of human cerebral cortex: solutions are in the surfaces. Proc Natl Acad Sci U S A 95:788–795.

Weinberger DR (1987): Implications of normal brain development for the pathogenesis of schizophrenia. Arch Gen Psychiatry 44: 660–669.

Wen W, Sachdev P, Shnier R, Brodaty H (2004): Effect of white matter hyperintensities on cortical cerebral blood volume using perfusion MRI. Neuroimage 21:1350–1356.

Wilke M, Kaufmann C, Grabner A, Putz B, Wetter TC, Auer DP (2001): Gray matter-changes and correlates of disease severity in schizophrenia: a statistical parametric mapping study. Neuroimage 13:814–824.